Morphological transition in compressible foam

D.L.Vainchtein and H.Aref

Department of Theoretical and Applied Mechanics, University of Illinois at Urbana-Champaign, 104 S. Wright St., Urbana, IL 61801, USA

Abstract

A theory to describe the morphological transition that occurs in a compressible foam when its volume is increased is constructed. The foam is observed to separate into two bubble populations or 'phases', one consisting of a large number of small bubbles, the 'liquid' phase, the other consisting of a small number of large bubbles, the 'gaseous' phase. First, working along lines similar to the van der Waals theory for a fluid system, approximate forms of the equation of state of the foam are derived and explored. These work well in the weakly compressible range, but fail to capture the nature of the transition. Taking a clue from the phenomenology, a theory of the 'phase separated' regime is then formulated working with the approximation that the two phases into which the foam separates are each relatively homogeneous. The successful single-phase formulae are applied to each phase, introducing an additional 'order parameter' which gives the ratio of the average size of bubbles in the two phases. Approximate expressions are written for the Helmholtz free energy and the equilibria of the foam derived from these. All results are compared to numerical simulations using Surface Evolver with very satisfying results. Due to the negligible size of thermal fluctuations, the morphological transition from a uniform to a non-uniform configuration as the system volume is expanded, is not spontaneous but consists of avalanches of reconnections with smooth evolution between them.

1 Introduction

In most papers on the mechanics of foams it is assumed that the gas within the bubbles is incompressible. As a result the condition that drives the evolution of the foam is

the minimization of the total area of the films constituting the boundaries between the bubbles subject to the constraint that the volume of each bubble is fixed. If we admit the compressibility of the gas, however, a dynamic balance arises between the elastic energy of the films and the compression of the gas within bubbles. Analogous phenomena occur in the study of magnetic froths ([1], [2]) but we shall use the context of a fluid system exclusively.

When the dynamic balance is pushed beyond some limit, foam morphologies that are quite different from those seen with incompressible foams arise. Indeed, as the role of the compressibility increases, a morphological or structural change of the equilibrium state of the foam, akin to a phase transition, is observed. For small compressibility all bubbles of the foam are of comparable sizes. As the compressibility of the foam becomes larger, a large number of the bubbles collapse and form clusters of very small bubbles which are then immersed in a background of a few very big bubbles. In the analogy to a phase transition, the clusters of small bubbles behave like a 'liquid' phase whereas the background of large bubbles behaves like a 'gaseous' phase. For convenience and ease of the numerical simulations we shall deal almost exclusively with the two-dimensional case in what follows. Thus, film 'area' will mean film 'length', bubble 'volume' will mean bubble 'area', and so on. All of the considerations in this paper carry over to three-dimensional systems, however.

In our previous paper [3] we derived the equation of state for compressible foam assuming ideal gas in all the bubbles. In the two-dimensional case this equation reads:

$$p_{ext}V + \frac{1}{2}\sigma A = NT, \tag{1}$$

Here V is the total area of the foam, A is twice the total length of all films between bubbles, N is the total number of gas molecules, T is the absolute temperature of the gas, assumed uniform over the foam, and σ is the surface tension, which is also assumed uniform throughout. In (1) and in the following we use the convention that temperature is measured in energy units, i.e., we set Boltzmann's constant to unity. Although (1) provides a relation between global characteristics of the foam, it says nothing about the detailed geometry of the bubbles, i.e., the distribution of bubble sizes or pressures. Numerical experiments show that these distributions undergo a drastic change as the effect of compressibility increases.

The balance between elastic energy in the films separating bubbles and the volume work required to compress a bubble can be quantified in various ways. A natural dimensionless parameter is provided by

$$\Lambda = \frac{\sigma A}{NT}. \tag{2}$$

Small values of Λ correspond to the more familiar incompressible foams that we encounter

in everyday experience with soap froths. Large values of Λ, on the other hand, correspond to the less familiar compressible foams that are the subject of study in this paper. The morphological transition described previously arises as Λ is increased from values somewhat less than unity to large values.

There are two important features of this system that distinguish it from most other thermodynamical systems in which we are used to discussing phase transitions. First, one cannot arbitrarily move bubbles around within the foam. Therefore, to describe a foam in equilibrium one must specify not only the properties of all the bubbles, but also their relative positions. A somewhat similar situation occurs in the case of granular media with grains of different shapes. Second, this system is almost free of naturally occurring fluctuations. Although the temperature of the foam is non-zero, thermal fluctuations are much too small to affect the geometry of the foam. As a result, this system provides an example of a non-entropy driven phase transition occurring at a non-vanishing temperature.

The outline of the paper is as follows. In section 2 we consider the Helmholtz free energy of the foam. First, we develop approximations for the weakly compressible regime. Then we present arguments as to why a geometrical change analogous to a phase transition occurs when Λ is varied across its range. In section 3 we first give a qualitative description of this geometrical instability. Then we introduce a model free energy, assuming the bubbles in the foam to come in just two sizes. We calculate the global minimum of this free energy for different values of the parameters and compare predictions of our model to numerical simulations results. In section 4 we discuss the transition from the uniform to a non-uniform configuration and comment on the role of fluctuations.

2 Helmholtz free energy

We can write Helmholtz's free energy in the form

$$F = -\sum_{i=1}^{M} N_i T \ln \frac{eV_i}{N_i} + \widehat{f}\,(N,T) + \sigma A, \tag{3}$$

$$= -NT\ln\frac{eV}{N} - \sum_{i=1}^{M} N_i T \ln\left(1 + \frac{\overline{p}_i V}{NT}\right) + \widehat{f}\,(N,T) + \sigma A, \tag{4}$$

where M is the total number of bubbles and $\overline{p}_i = p_i - NT/V$ is the difference between the pressure in the i-th bubble and the volume-weighted average of bubble pressures NT/V: $(1/V)\sum_{i=1}^{M} V_i p_i = NT/V$. The function $\widehat{f}\,(N,T)$ is a known function of N and T for a given ideal gas (see [4]). The first two terms in (3) are the contribution of the ideal gas.

The last term is the surface energy of the films between the bubbles. As N and T are kept constant throughout our discussion, we omit $\widehat{f}(N,T)$ below.

We can expand the logarithm on the right hand side of (4) to get

$$\begin{aligned} F &= F_0 + \sum_{i=1}^{M} N_i T \sum_{k=1}^{\infty} \frac{(-1)^k}{k} \left(\frac{\overline{p}_i V}{NT}\right)^k + \sigma A, \\ &= F_0 + \frac{NT}{V} \sum_{k=2}^{\infty} \frac{(-1)^k}{k(k-1)} \left[\sum_{i=1}^{M} V_i \left(\frac{\overline{p}_i V}{NT}\right)^k\right] + \sigma A, \end{aligned} \tag{5}$$

where $F_0 = -NT\ln\frac{eV}{N}$ is the Helmholtz free energy of N molecules of ideal gas in a box of volume V. Going from the first line to the second in (5) we changed the order of summation and substituted $N_i T = V_i\left(\overline{p}_i + NT/V\right)$. Terms in square brackets in the last line in (5) can be considered to be moments of the volume-weighted pressure distribution of the given state of the foam. These moments characterize the state of the foam. All $\overline{p}_i$'s are zero if all bubbles are identical and, of course, also in the case of vanishing surface tension.

The expression for A can be obtained by differentiating (5) with respect to V, to obtain p_{ext}, and comparing to the equation of state (1). It was shown in [3] that

$$\sigma A = f\left(\sigma V^{1/2}\right), \tag{6}$$

where f is an unknown function, the form of which must be determined from consideration of the exact configuration of the foam. Equation (5) when differentiated essentially provides an expansion for f in terms of moments of bubble pressure distribution.

In the remainder of this section we consider what we call a 'weakly compressible regime' – when the compressibility of the gas can be considered as a perturbation. In this case different approximations can be obtained by taking into account different numbers of terms in the expansion (5). We discuss the two simplest approximations (keeping no terms and one term, respectively) and we discuss the differences between these two approximations.

In the first approximation all the terms with over-bars in (5) are neglected and for A we get

$$A = \nu V^{1/2},$$

where ν is a constant for a given foam. The equation of state becomes

$$p_{ext}V + \frac{1}{2}\sigma\nu V^{1/2} = NT. \tag{7}$$

The value of ν can be calculated once at some point of the (p_{ext}, V) diagram. When the distribution of bubble sizes is rather narrow, the scaling of ν with the number of bubbles is given by

$$\nu \approx \nu_1 M^{1/2}, \tag{8}$$

where ν_1 does not depend on the number of bubbles and may be thought of as an average value of the ratio of the length of the films, constituting the boundary of a bubble, to the square root of the area of that bubble. For a circle this value would be approximately 3.54. A typical value of ν_1 in our numerical simulations is between 3.7 and 4.0 depending on the nature of the foam generated. The estimate (8) becomes invalid when the differences between pressures in different bubbles become comparable to the pressures themselves.

The (p_{ext}, V) diagram of the approximate equation of state (7) is shown in Figure 1 for different values of σ for foams with the same values of N, T, and ν. This is the same diagram shown in [3] (Figure 2). One can see that all the curves in Fig.1 for non-vanishing σ contain a portion with $p_{ext} < 0$. Although $p_{ext} < 0$ has no physical meaning for a foam that is surrounded by gas at pressure p_{ext}, this situation can be realized by placing the foam in a container. In this case $p_{ext} < 0$ signifies that the net force per unit area exerted by the walls of the container on the foam is directed outward.

The other notable feature of these curves is that each of them (for $\sigma > 0$) has a minimum located at

$$V_{cr} = 16\left(\frac{NT}{\sigma\nu}\right)^2, \quad p_{cr} = -\frac{NT}{V_{cr}}. \tag{9}$$

In terms of V_{cr} and p_{cr} the approximate equation of state (7) may be written as

$$\frac{p_{ext}}{|p_{cr}|} = \frac{V_{cr}}{V}\left(1 - 2\left(\frac{V}{V_{cr}}\right)^{1/2}\right). \tag{10}$$

The existence of the minimum is important since in classical thermodynamics an intrinsic stability criterion for any system is

$$\left(\frac{\partial p_{ext}}{\partial V}\right)_{N,T} < 0.$$

The physical meaning of this condition is that unless this inequality is satisfied, the system will spontaneously contract. In the case of a foam in a container the volume

(area in 2D) of the foam is given. Hence, assuming the foam continues to adhere to the walls of the container, the instability cannot manifest itself by contraction of the foam as a whole: loss of stability must result in a spontaneous loss of uniformity of the bubble distribution (and, thus, all the assumptions made in arriving at the approximate equation of state (7) become invalid). This explains why numerical experiments show that (7) and (8) hold rather well only for small to moderate values of the foam volume, for $V \lesssim V_{cr}$, where V_{cr} is given by (9). At some critical volume the foam undergoes a drastic change in the distribution of bubble sizes as the uniform configuration becomes unstable, making (7) and (8) invalid for $V \gg V_{cr}$. In this sense V_{cr} plays the role of a reference volume: when the volume of the foam is said to be 'large' or 'small', it is with respect to V_{cr}. Going back to the dimensionless parameter Λ defined in (2), and using (9), we see that $\Lambda = 4(V/V_{cr})^{1/2}$. Since the approximate equation of state (7) signals an instability, the portions of the curves in the (p_{ext}, V) diagram for which $V > V_{cr}$ are shown by dashed lines.

For $V < V_{cr}$ one can improve the approximate equation of state (7) by taking into account further terms from the moment expansion (5). In 2D the term that corresponds to $k = 2$ in (5) is proportional to $\sigma^2 V$. This estimate follows from the argument that the $\overline{p}_i$'s are of the order of the pressure difference between adjacent bubbles which, in turn, are of order $\sigma/V^{1/2}$, since to leading order the radius of curvature of a film scales as the square root of the volume. The same scaling could be obtained from (6) if we assume that the function f is analytic.

Hence, the improved approximations to F and A in terms of V are

$$F = F_0 + \beta \frac{1}{NT} \sigma^2 V + \sigma A; \quad A = \nu V^{1/2} - 2\beta \frac{1}{NT} \sigma V. \tag{11}$$

For a given foam β is a constant in the same sense that ν is a constant. Once ν is calculated (and it is now clear that it is best to calculate ν for small V) β can be calculated. One can readily see from the second line in (5) that β is positive and is proportional to the number of bubbles, M. Substituting the expression for A from (11) into (1) we get the next approximation for the equation of state:

$$p_{ext} V + \frac{1}{2} \sigma \nu V^{1/2} - \sigma^2 \beta \frac{1}{NT} V = NT, \tag{12}$$

or, in terms V_{cr} and p_{cr},

$$\frac{p_{ext}}{|p_{cr}|} = \frac{V_{cr}}{V} \left(1 - 2 \left(\frac{V}{V_{cr}} \right)^{1/2} \right) + 16 \frac{\beta}{\nu^2}. \tag{13}$$

Note, that the last term in (13) is independent of M.

We performed a set of numerical simulations using the 'Surface Evolver' code package [6]. Figures 2a and 2b display (p_{ext}, V) curves for constant values of surface tension, N, and T, for a foam with a free boundary and for a foam subject to periodic boundary conditions, respectively. Squares denote values of p_{ext} obtained from the simulations. (In the case of periodic boundary conditions p_{ext} has no independent meaning, so it was calculated using the exact equation of state (1) in which all other quantities are either set or can be found from the simulation.) Dashed curves are the values of p_{ext} calculated using equation (10) and solid curves are the values of p_{ext} calculated using equation (13). The parameters ν and β were determined using the portion of the (p_{ext}, V) curve for very small values of V. We see that the approximation (10) is reasonably accurate. Taking into account one more term, which in 2D just shifts the curve up since the term proportional to β corresponds to an additive pressure, improves the accuracy for $V \approx V_{cr}$ considerably. Note, that in 2D the term proportional to β does not change the value of V_{cr}, while slightly changing (increasing) the value of volume at which the curve intersects the line $p_{ext} = 0$, V_0. The values determined for ν_1 and β were different for the free-boundary and the periodic-boundary-condition foams. For the free-boundary foam the comparison had to be stopped when the external pressure approached zero, which happens at V slightly larger then V_0. In spite of this for the sake of consistency we kept the normalization used in (13) and (10). For the periodic-boundary-condition foam it was possible to extend the simulation all the way past V_{cr}, indeed, somewhat into the intrinsically unstable region. The approximate equation of state in the form (13) continued to hold with remarkable accuracy. Figures 3a and 3b show typical views of these two simulated foams.

We remark on the similarity of this approach to improve the approximate equation of state to van der Waals' improvement of the equation of state of an ideal gas (cf. [4]). Just as the quantity b in van der Waals theory – the excluded volume per molecule – is approximately four times the volume of a molecule for monatomic gases, so is ν_1 approximately the ratio of the length of the boundary of a bubble, to the square root of the area of that bubble. The exact value of ν_1 and β, like the values of a and b in van der Waals theory, must be fit by comparison to empirical data.

3 Model free energy for two types of bubbles

Figures 4a–d show a foam consisting of 1000 bubbles with periodic boundary conditions for four different values of the total volume V. Figure 3a corresponds to a small value of V in the sense of Section 2, $V \ll V_{cr}$. Figure 4b corresponds to an intermediate value of V, V slightly above V_{cr}. Figure 4c corresponds to a still larger value of V, and Figure 4d corresponds to a large value of V, $V \gg V_{cr}$. It is clear from Figs.4b–d that for large values of V the distribution of bubble sizes is not uniform. Figure 5 shows the 'measured'

frequency distribution of bubble pressures for configurations shown in Figs.4a (Fig.5a) and 4b (Fig.5b). The transition from a one-peak distribution in Fig.5a to a two-peak distribution in Fig.4b suggests an analogy with a first order gas-liquid phase transition (cf. [7]). In this analogy each peak corresponds to a phase. We shall think of the low-pressure peak as the 'gaseous' phase, and the high-pressure peak as the 'liquid' phase. The appearance of two peaks signals that for large V the expansion in (5) cannot be used. On the other hand, it also suggests an approach to describing the 'phase-separated' foam in which we explicitly realize that there are two types of bubbles. We now explore a theory along these lines.

Consider, then, the following model. Assume the foam consists of bubbles of just two types, some that are relatively large and some that are relatively small. Such a description requires a new parameter to describe the relative position of the two maxima in Fig.5b. Since in any bubble by the ideal gas equation of state $p_i = \rho_i T$, where ρ_i is the density of the gas, the ratio of pressures at the maxima equals the ratio of typical densities.

To construct our theory we will use the developments in section 2 within each of the two bubble populations or 'phases'. Hence, we introduce the following quantities: M_g, N_g, V_g, and ν_g, to denote the values of M, N, V and ν for the 'gaseous' phase. Similarly, M_l, N_l, V_l, and ν_l denote these quantities for the 'liquid' phase. The intensive variables $n_g = N_g/M_g$, $v_g = V_g/M_g$, $n_l = N_l/M_l$, and $v_l = V_l/M_l$ will also prove useful.

It will become clear that we always have $M_g \ll M_l$. The approximately uniform configurations discussed in section 2 correspond to $M_g = 0$, $M_l = M$. We wish to find conditions for when the approximately uniform configurations cease to correspond to the global minimum of the free energy of the system.

Assuming that bubbles within each 'phase' are identical (in other words we assume that the difference between bubbles within a 'phase' is small compared to the difference between any two bubbles chosen one from either 'phase'), we can use the relations from section 2:

$$A_g = \nu_g V_g^{1/2} = M_g^{1/2} \nu_{1,g} V_g^{1/2}; \quad A_l = \nu_l V_l^{1/2} = M_l^{1/2} \nu_{1,l} V_l^{1/2}. \tag{14}$$

We distinguish the values of ν_1 for the two 'phases' since, as is clear from Figs.4c and 4d, the shapes of the bubbles in the two 'phases' are quite different – the bubbles in the 'liquid' phase are rounded with all sides approximately the same length (thus resembling bubbles in a uniform configuration), the bubbles in the 'gaseous' phase may also be rounded, but sometimes they are long and thin (see Fig.4c). Due to the large differences between the two types of bubbles, (8) is now not valid for the foam as a whole. Substituting (14) into (3) we obtain

$$F = \sum_{x=g,l} \left(-M_x n_x T \ln \frac{e v_x}{n_x} + \sigma M_x \left(\nu_{1,x} v_x^{1/2} \right) \right), \tag{15}$$

with the normalizing conditions $M_g + M_l = M$, $M_g v_g + M_l v_l = V$, and $M_g n_g + M_l n_l = N$. For given values of M, N, V, and σ we can consider the free energy F to be a function of just three variables:

$$F = F\left(\frac{v_g}{v_l}, \frac{M_g}{M_l}, \frac{n_g}{n_l}\right). \tag{16}$$

Equilibria of the two-phase foam correspond to minima of F. The ratio n_g/n_l depends on M_g/M_l and on the distribution of gas molecules among the bubbles, since it is reasonable to assume that larger bubbles contain more particles and that such bubbles are more likely to expand (i.e., end up in the 'gaseous' phase). Numerical simulations show that quantitative properties of the parametric evolution of the foam do depend on the distribution of gas particles among bubbles. On the other hand, overall qualitative properties of the free energy, e.g., whether it has one or more minima, are independent of this distribution. Therefore, for the remainder of this section we shall ignore the dependence of F on n_g/n_l and return to it in Section 4.

We introduce a parameter $\varphi = v_g/v_l$, that gives the ratio of sizes of a typical bubble in the two phases. It will become clear below that this parameter is more convenient than a more common choice such as $\overline{\varphi} = (v_g - v_l)/(v_g + v_l)$. Of course, these two parameters are equivalent: $\overline{\varphi} = 0$ when $\varphi = 1$ and $\overline{\varphi} = 1$ as $\varphi \to \infty$. In our model φ plays the role of an *order parameter*. If the typical number of gas particles in each bubble of either phase is of the same order, then φ gives also the ratio of typical pressures between bubbles in these two phases.

Figure 6 presents schematic plots of $F = F(\varphi)$ for different values of V. Consider starting from some small value of V for which $\varphi = 1$ (uniform configuration) is the only minimum of F and then gradually increasing V. At some critical value V_* a secondary minimum, located at $\varphi = \varphi_*$, appears. At $V = V_*$ we have

$$\left.\frac{\partial F}{\partial \varphi}\right|_{\varphi=\varphi_*} = \left.\frac{\partial^2 F}{\partial \varphi^2}\right|_{\varphi=\varphi_*} = 0.$$

As we increase V beyond V_*, the value of $F(\varphi_*)$ decreases. For $V_* < V < V_{**}$ the uniform configuration is still the global minimum: $F(\varphi = 1) < F(\varphi_*)$. A second critical volume V_{**} arises when the condition $F(\varphi = 1) = F(\varphi_*)$ is met. For $V > V_{**}$ the minimum at $\varphi = 1$ remains as a local minimum (i.e., the uniform configuration is metastable). This remains true until V reaches the third critical volume $V = V_{***}$, at which point $\varphi = 1$ becomes a point of local maximum of F. Hence, for large volumes the energetically preferred configuration is not uniform, but consists of a few very large bubbles and many small bubbles.

The values of the first two critical volumes, V_* and V_{**}, may be found numerically. The value of the third critical volume V_{***} is given by

$$\left.\frac{\partial^2 F}{\partial \varphi^2}\right|_{\varphi=1} = 0. \tag{17}$$

Substituting the definition of φ and (16) into (17) we obtain

$$V_{***} \approx \left[\frac{4NT}{\sigma \nu_{1,l}\sqrt{M}}\right]^2.$$

It is reasonable to assume that the value of $\nu_{1,l}$ is approximately equal to ν_1 for the uniform configuration of the same foam: $\nu_{1,l} \approx \nu_1$. Therefore, we arrive at (see (9))

$$V_{***} \approx V_{cr}.$$

Numerical simulations show that when the foam phase separates, it settles into a configuration with a fixed number of large bubbles, M_g, and this state of affairs remains for some considerable range of further increase in volume. One can easily check (see also Figure 7 below) that the value of F at the secondary minimum φ_* increases as M_g increases. Hence the global minimum of F corresponds either to the uniform configuration, or to the non-uniform configuration with $M_g = 1$. States with $M_g > 1$, although not the most energetically preferable, correspond to a relative minimum of F and thus may be realized in practice for some range of the parameters. We return to this issue in Section 4.

The values of φ_* are of order M. Therefore, for large M the density of gas in the small bubbles (of the 'liquid' phase) is much larger than the density in the large bubbles (of the 'gaseous' phase). This is why we refer to the phase of small bubbles as 'liquid' and the phase of large bubbles (or, in the absolute minimum of free energy, a single bubble) as 'gaseous'.

Let us discuss some properties of foam when $V \gg V_{***}$ or, equivalently, for very large Λ. For each value of M_g we can find an asymptotic value of φ_*. From the minimum condition

$$\left.\frac{\partial F}{\partial \varphi}\right|_{\varphi=\varphi_*} = 0,$$

we get

$$1 + M_g \frac{\varphi_*}{M} \approx \frac{V}{V_0}, \tag{18}$$

where $V_0 = 4\left(NT/\sigma\nu\right)^2 = V_0/4$ is the volume that corresponds to $p_{ext} = 0$ when calculated using (7). V_0 is of the order of the largest possible value of volume for a free boundary foam (i.e. a foam that is surrounded by air, see Section 2).

It follows from the definition of φ that for $M_g \ll M$ the volume of the liquid phase, V_l, is

$$V_l \approx M \frac{V}{M + M_g \varphi_*}. \tag{19}$$

Therefore, once a foam comes into a non-uniform state, the volume of the liquid phase remains nearly constant, $V_l \cong V_0$, as we increase the total volume of the foam, regardless of the value of M_g. Hence, in the first approximation the liquid phase is incompressible, just like an ordinary liquid!

The last result could be obtained without any calculation just by noticing that a typical pressure in the liquid phase is much higher than a typical pressure in the gaseous phase. Therefore, for clusters of bubbles in the liquid phase the background of the gaseous phase appears approximately as vanishing ambient pressure.

Note, that it follows from the definition of V_0 and the scaling assumption (8) that V_0 is proportional to M. Hence, the total volume of the liquid phase is always approximately equal to V_0, regardless of how many clusters it is divided into.

The above considerations also provide a way to improve the estimate of V_l. If we approximate the free energy using (11), we readily get a more accurate (slightly larger) value of V_l.

One can show that all the critical volumes, V_{cr}, V_*, V_{**}, and V_{***}, are larger then V_0. Therefore, all free boundary foams are in the uniform state.

4 The role of fluctuations

In a general thermodynamic system we rely on thermal fluctuations to drive the system towards the global minimum of F. In the case of a foam, thermal fluctuations are much too small to play this significant role, and we must appeal to other kinds of fluctuations to drive the system to equilibrium.

In our considerations in the preceding sections we have ignored the diffusion of gas between bubbles, which provides some level of fluctuation. All that remains is the 'noise' associated with the criterion of reconnection of bubble films, which, in turn, models several physical phenomena at the microscopic scale. In the absence of fluctuations the foam will relax to one of many local minima instead of the global minimum. The exact characteristics of a given local minimum depend not only on the parameters of the whole system, but also on the way the system was produced, i.e., on the initial state.

There are, at least, two scales of length and energy in the problem that need to be recognized: the small scale is associated with single bubbles; the large scale pertains to the foam as a whole. The global structure of the free energy described in the previous section depends on the large scale. The fine structure of small local minima, where every

local minimum of free energy corresponds to an equilibrium configuration of the foam, is imposed on this large scale structure. The very existence of this fine structure is dictated by Plateau's rules and the Young-Laplace law, which tell us that any two configurations are separated by a local maximum. In usual thermodynamic systems fluctuations smooth these local minima leaving only the large-scale structure. In our case thermal fluctuations are too small to force rearrangements in the foam, i.e., a jump from one configuration to another, even if the second configuration has less energy than the first.

In our calculations we have concentrated on parametric changes. Because of the scaling, as discussed in [3], a change in any parameter can be put into correspondence with a change of volume and so we may restrict our discussion to this case. If the foam volume is being changed stepwise, then the size of the step defines an amplitude of 'fluctuation': a change of volume pushes the system away from equilibrium and then the system relaxes towards a new equilibrium.

Another source of fluctuations is spontaneous reconnection. In the process of evolution of the foam some edges may become relatively short (compared with the neighboring ones). This generally leads to what is known as a T1 event. These reconnections can increase or decrease the energy, although usually the elimination of short edges reduces the energy. This is similar to the phenomenology of shaking a container filled with a relatively dense packed granular material. All these mechanisms provide a level of fluctuations of order of the energy per bubble, while the transition from a uniform to a non-uniform state requires rearrangements on the scale of the whole foam. As a result, while the transition from a uniform to a non-uniform state typically occurs when the free energy of the non-uniform state becomes equal to the free energy of the uniform state, in our case this transition may be delayed due to the absence of fluctuations of the required size. This kind of the behavior distinguishes the foam from most thermodynamic systems.

If we start with a small value of volume (i.e., a small value of Λ) and proceed to gradually increase the volume, the foam remains rather uniform all the way to V_{***}. Even beyond V_{***} the transition to a highly non-uniform configuration with some small value of M_g is not immediate, as it requires a global rearrangement of the foam. Thus, what in theory is a sharp, first-order phase transition (i.e., an immediate jump of M_g to some small value or, in terms of notation of Section 3, a large jump in φ), will in numerical experiments looks more like a sequence of such transitions.

The initial jump of M_g to some relatively large value is followed by a gradual decrease of M_g (by a sequence of small changes) with smooth evolution between them (at constant M_g). Figure 7 shows the free energy (normalized by NT) in a numerical simulation of the foam as the volume is gradually increased ('forward evolution', squares) and then decreased from the terminal state ('backward evolution', circles). Each drop of free energy along the upper curve (increasing volume) corresponds to a rearrangement of the foam that decreases M_g by 1. Sometimes one rearrangement stimulates an entire avalanche of

rearrangements. The general tendency of the free energy to increase with volume between reconnections reflects the surface energy increasing faster than the ideal gas energy decreases. The thin curves in Fig.7 correspond to values of the free energy computed using the two-phase model discussed in Section 3 with $M_g = 2$ (lower curve), $M_g = 3$ (middle curve), and $M_g = 4$ (upper curve). Figure 8a–d illustrates the sequence of reconnections that occur between $V/V_{cr} = 6$ and $V/V_{cr} = 10$. In Fig.8a there are, clearly, some big bubbles, there are small bubbles, and also several bubbles of intermediate size. As we go from Fig.8a (which correspond to point A in Fig.7) to Fig.8b (point B in Fig.7) and on to Figs.8c (point C) and 8d (point D), the number of big bubbles, M_g, decreases from 4 to 3 to 2, and the bubbles of intermediate size shrink.

One can see that the curve corresponding to decreasing volume is smoother then the one for increasing volume, since once settled in the state with $M_g = 2$, the system stays there nearly all the way to V_*, and its free energy can be well approximated by the two-phase model. This behavior is illustrated in Fig.9, which shows a magnified part of some of Fig.7, corresponding to small values of V. We see a hysteresis-like effect: points corresponding to 'backward evolution' lie well above points, that correspond to 'forward evolution'.

Acknowledgement

This work was supported by the NASA Microgravity Fluid Physics program under grant NASA NAG3-2122.

References

[1] D.Weaire, F.Bolton, P.Molho, and J.A.Glazier, Investigation of an elementary model for magnetic froth. *J.Phys.: Condens. Matter* **3**, 2101-2114 (1991).

[2] K.L.Babcock, and R.M.Westerwelt, Elements of cellular domain patterns in magnetic garnet films. *Phys. Rev. A*, **40**, 4, 2022-2037 (1989).

[3] H.Aref and D.Vainchtein, The equation of state of a foam. *Physics of Fluids* **12**, 1, 23-28 (2000).

[4] L.D.Landau and E.M.Lifschitz, *Statistical Physics.* Pergamon (1980).

[5] T.Herdtle, PhD thesis, University of California, San Diego (1991), 65pp.

[6] K.A.Brakke, The Surface Evolver. *Exper. Math.* **1**, 141-165 (1992).

[7] M.Rovere, D.W.Heermann, and K.Binder, The gas-liquid transition of the two-dimensional Lennard-Jones fluid. *J. Phys.: Condens. Matter* **2**, 7009-7032 (1990).

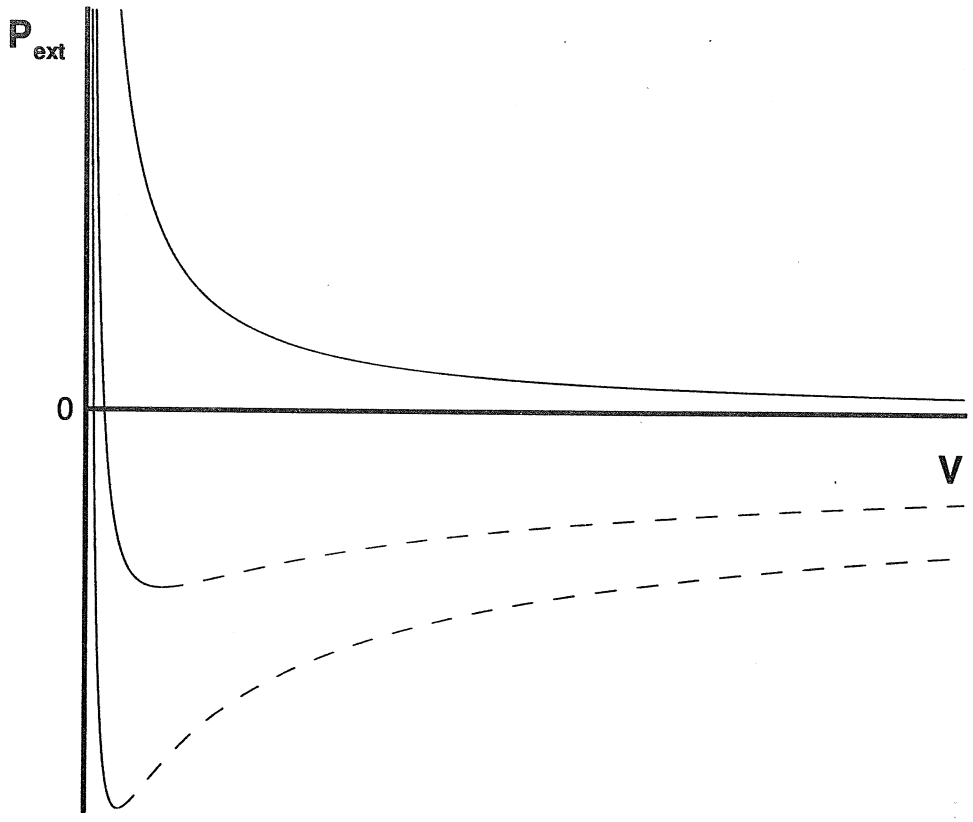

Figure 1: (p_{ext}, V) diagram of the approximate equation of state (7) for different values of σ. The same values of N, T, and ν are the same for all the curves.

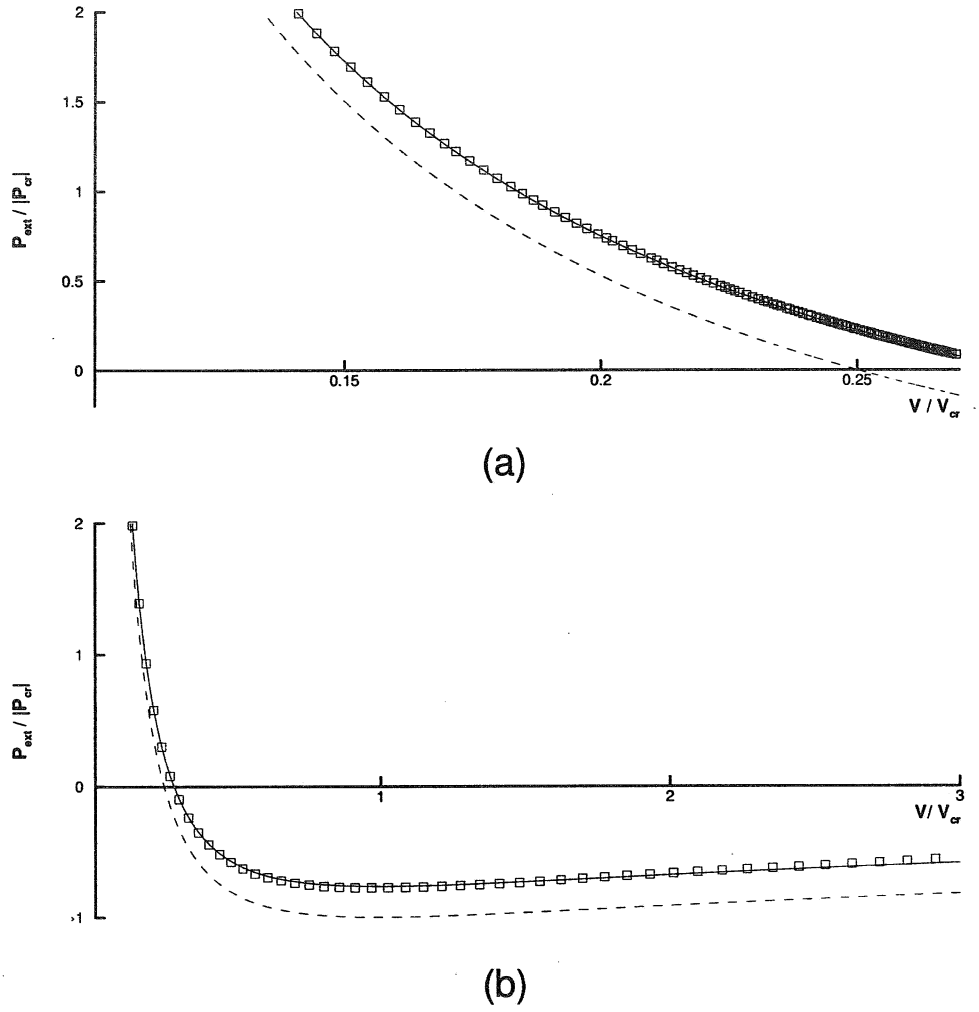

Figure 2: (p_{ext}, V) diagrams for 'weakly compressible regime': (a) a free boundary foam, consisting of 96 bubbles, and (b) a foam subject to periodic boundary conditions, consisting of 1000 bubbles. Squares denote values of p_{ext} obtained from simulations. Dashed curves give the value of p_{ext} calculated using equation (10) and solid curves are the values of p_{ext} calculated using equation (13).

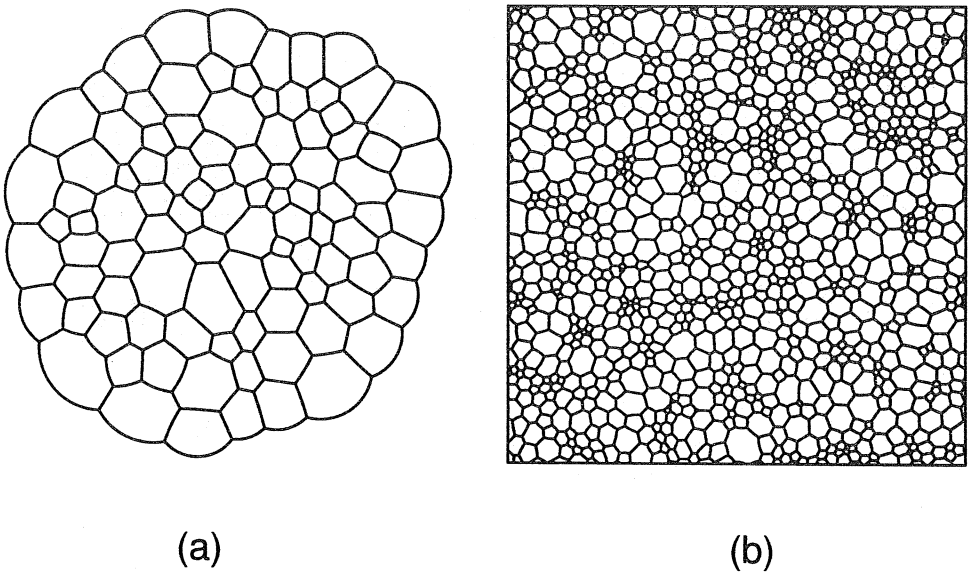

Figure 3: Typical view of (a) a free boundary foam, and (b) a foam subject to periodic boundary conditions.

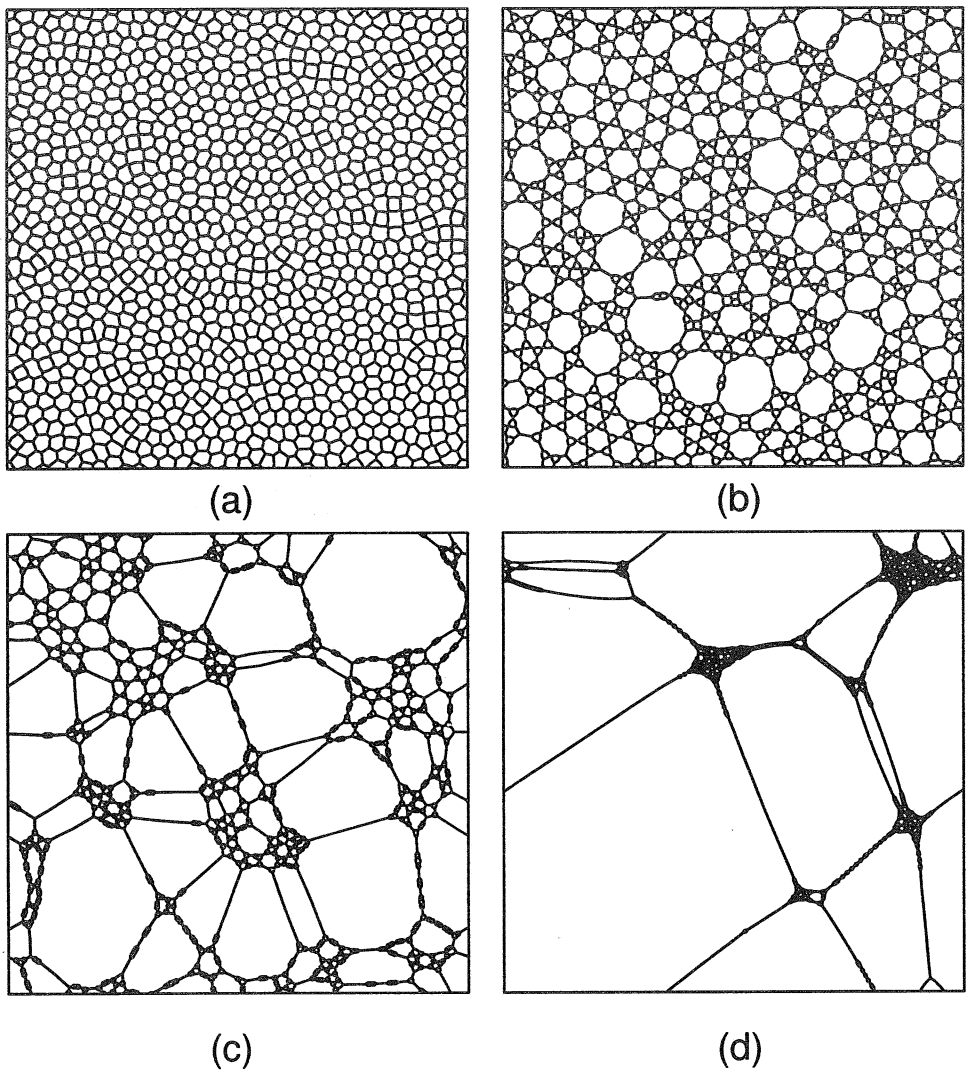

Figure 4: Snapshots of a foam consisting of 1000 bubbles for different values of volume. The volume increases through the sequence a, b, c, d.

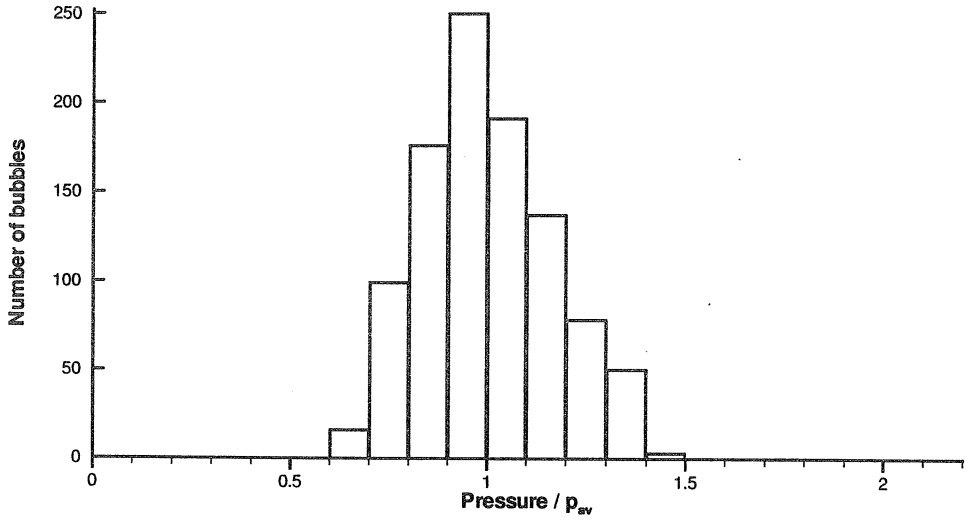

(a)

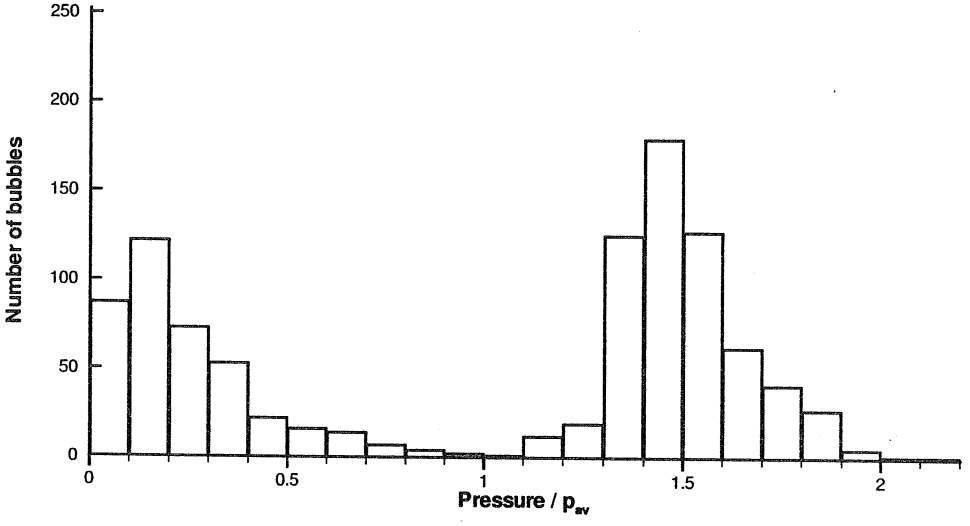

(b)

Figure 5: Distributions of bubble pressures for a foam, consisting of 1000 bubbles in different stages of evolution. Pressure is normalized by the average pressure, $p_{av} = 1/M \sum_{i=1}^{M} p_i$; (a) uniform configuration, $V \ll V_{cr}$, (b) non-uniform configuration, $V > V_{cr}$.

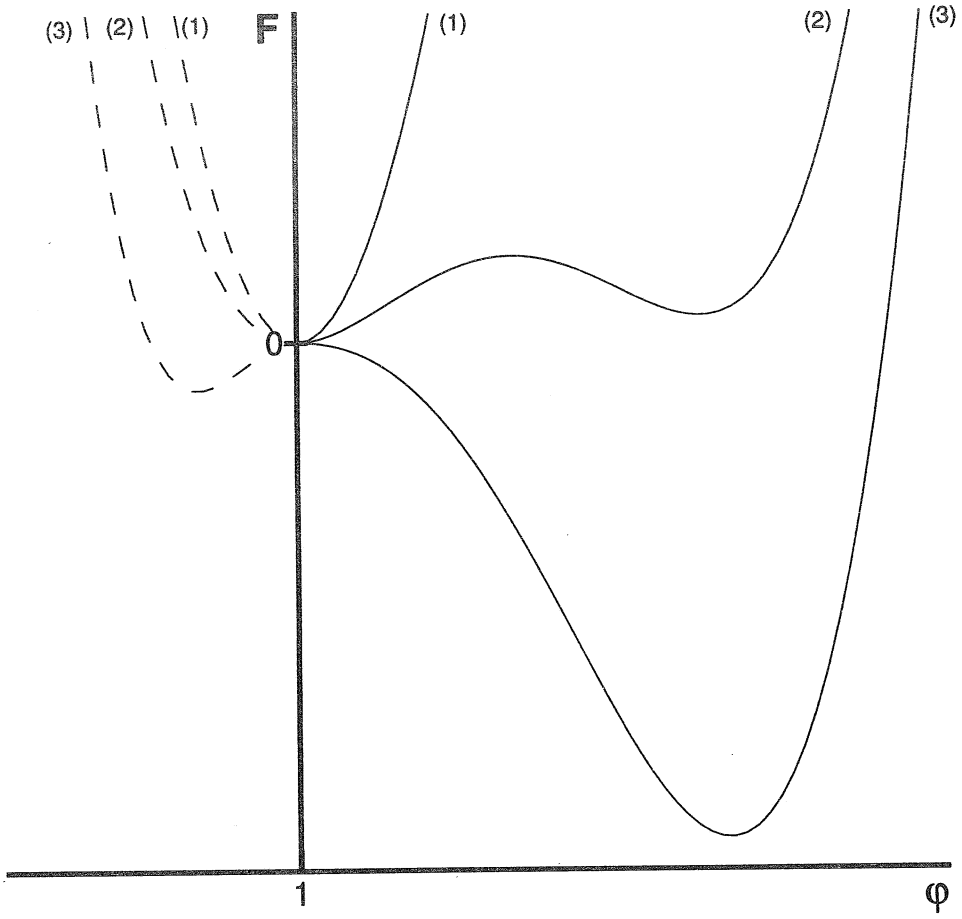

Figure 6: Schematic plot of $F = F(\varphi)$ for different values of V. (1) $V < V_*$; (2) $V_* < V < V_{**}$; (3) $V_{***} < V$.

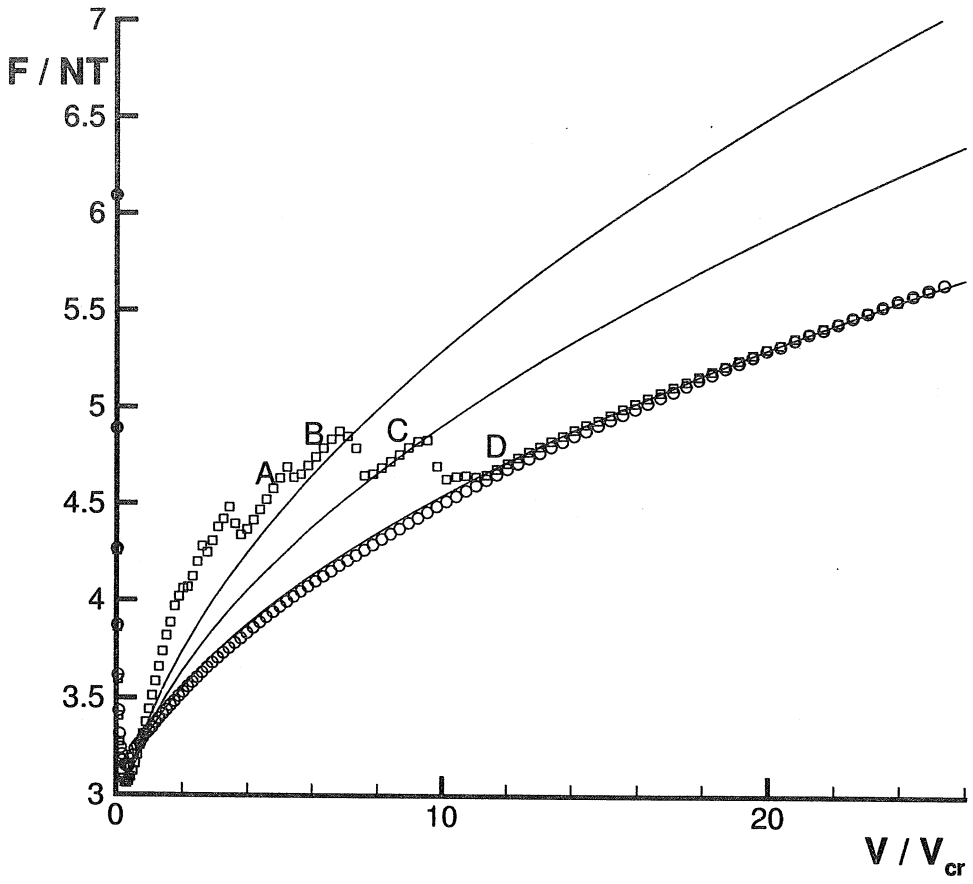

Figure 7: Free energy as a function of order parameter for the numerical simulation of a foam when the volume is gradually increased (squares) and then decreased (circles) from the terminal state. The thin curves correspond to the values of free energy computed using the two-phase model discussed in Section 3 with $M_g = 2$ (lower curve), $M_g = 3$ (middle curve), and $M_g = 4$ (upper curve). The volume of the foam is normalized by V_{cr}.

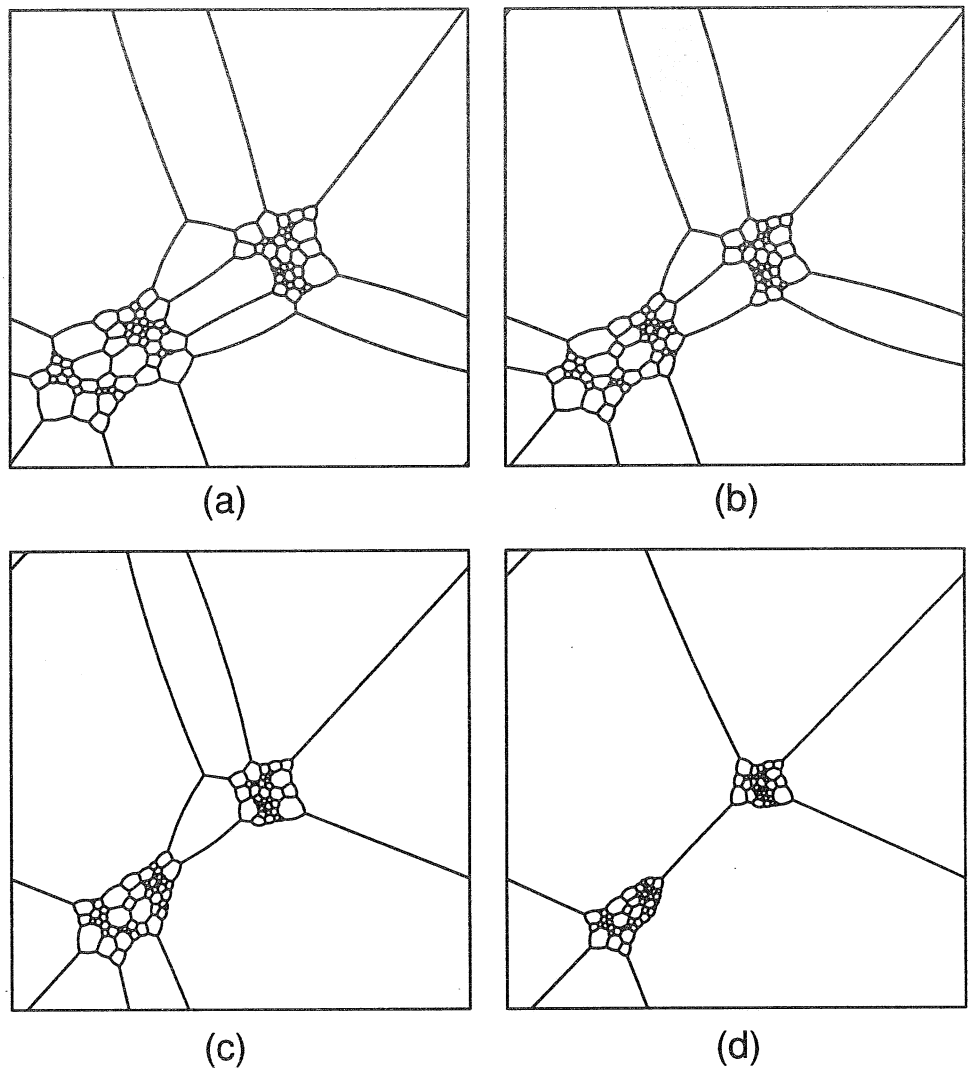

Figure 8: Snapshots of the foam in the process of 'forward evolution' between $V/V_{cr} = 6$ and $V/V_{cr} = 10$. As we go from Fig.8a (point A on Fig.7) to Fig.8b (point B) to Fig.8c (point C) to Fig.8d (point D) the number of big bubbles, M_g, decreases from 4 to 3 to 2 and the bubbles of the intermediate size shrink.

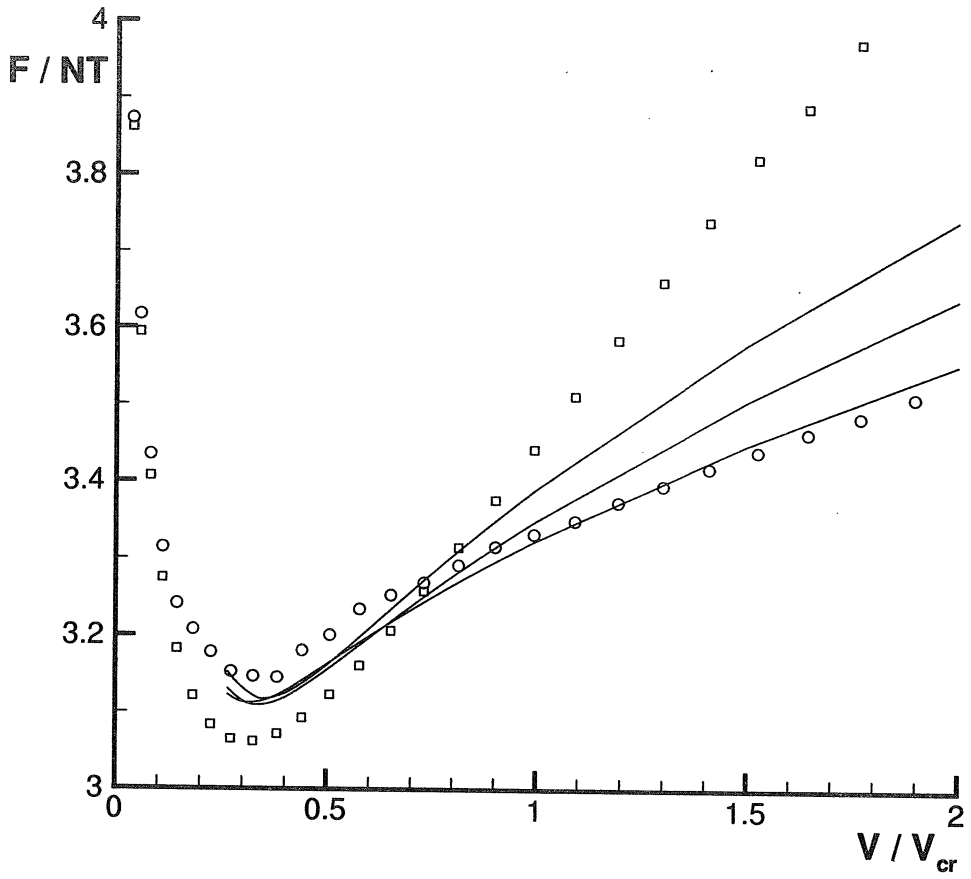

Figure 9: Same as Figure 7, with the portion $V/V_{cr} < 2$ magnified to illustrate the hysteresis.

List of Recent TAM Reports

No.	Authors	Title	Date
860	Najjar, F. M., and S. Balachandar	Low-frequency unsteadiness in the wake of a normal plate, *Bulletin of the American Physical Society* **42**, 2212 (1997)	Aug. 1997
861	Short, M.	A parabolic linear evolution equation for cellular detonation instability—*Combustion Theory and Modeling* **1**, 313–346 (1997)	Aug. 1997
862	Short, M., and D. S. Stewart	Cellular detonation stability, I: A normal-mode linear analysis—*Journal of Fluid Mechanics* **368**, 229–262 (1998)	Sept. 1997
863	Carranza, F. L., and R. B. Haber	A numerical study of intergranular fracture and oxygen embrittlement in an elastic–viscoplastic solid—*Journal of the Mechanics and Physics of Solids*, **47**, 27–58 (1997)	Oct. 1997
864	Sakakibara, J., and R. J. Adrian	Whole-field measurement of temperature in water using two-color laser-induced fluorescence—*Experiments in Fluids* **26**, 7–15 (1999)	Oct. 1997
865	Riahi, D. N.	Effect of surface corrugation on convection in a three-dimensional finite box of fluid-saturated porous material—*Theoretical and Computational Fluid Dynamics*, 13, 189-208 (1999)	Oct. 1997
866	Baker, C. F., and D. N. Riahi	Three-dimensional flow instabilities during alloy solidification—*Bulletin of the American Physical Society* **41**, 1699 (1998)	Oct. 1997
867	Fried, E.	Introduction (only) to *The Physical and Mathematical Foundations of the Continuum Theory of Evolving Phase Interfaces* (book containing 14 seminal papers dedicated to Morton E. Gurtin), Berlin: Springer-Verlag, in press (1998)	Oct. 1997
868	Folguera, A., and J. G. Harris	Coupled Rayleigh surface waves in a slowly varying elastic waveguide—*Proceedings of the Royal Society of London A* **455**, 917–931 (1998)	Oct. 1997
869	Stewart, D. S.	Detonation shock dynamics: Application for precision cutting of metal with detonation waves	Oct. 1997
870	Shrotriya, P., and N. R. Sottos	Creep and relaxation behavior of woven glass/epoxy substrates for multilayer circuit board applications—*Polymer Composites* **19**, 567–578 (1998)	Nov. 1997
871	Riahi, D. N.	Boundary wave–vortex interaction in channel flow at high Reynolds numbers, *Fluid Dynamics Research* **25**, 129–145 (1999)	Nov. 1997
872	George, W. K., L. Castillo, and M. Wosnik	A theory for turbulent pipe and channel flows—paper presented at *Disquisitiones Mechanicae* (Urbana, Ill., October 1996)	Nov. 1997
873	Aslam, T. D., and D. S. Stewart	Detonation shock dynamics and comparisons with direct numerical simulation—*Combustion Theory and Modeling* **3**, 77–101 (1999)	Dec. 1997
874	Short, M., and A. K. Kapila	Blow-up in semilinear parabolic equations with weak diffusion *Combustion Theory and Modeling* **2**, 283-291 (1998)	Dec. 1997
875	Riahi, D. N.	Analysis and modeling for a turbulent convective plume—*Mathematical and Computer Modeling* **28**, 57–63 (1998)	Jan. 1998
876	Stremler, M. A., and H. Aref	Motion of three point vortices in a periodic parallelogram—*Journal of Fluid Mechanics* **392**, 101-128 (1999)	Feb. 1998
877	Dey, N., K. J. Hsia, and D. F. Socie	On the stress dependence of high-temperature static fatigue life of ceramics	Feb. 1998
878	Brown, E. N., and N. R. Sottos	Thermoelastic properties of plain weave composites for multilayer circuit board applications	Feb. 1998
879	Riahi, D. N.	On the effect of a corrugated boundary on convective motion—*Journal of Theoretical and Applied Mechanics*, in press (1999)	Feb. 1998
880	Riahi, D. N.	On a turbulent boundary layer flow over a moving wavy wall	Mar. 1998
881	Riahi, D. N.	Vortex formation and stability analysis for shear flows over combined spatially and temporally structured walls—*Mathematical Problems in Engineering* **5**, 317–328 (1999)	June 1998
882	Short, M., and D. S. Stewart	The multi-dimensional stability of weak heat release detonations—*Journal of Fluid Mechanics* **382**, 109–135 (1999)	June 1998

List of Recent TAM Reports (cont'd)

No.	Authors	Title	Date
883	Fried, E., and M. E. Gurtin	Coherent solid-state phase transitions with atomic diffusion: A thermomechanical treatment—*Journal of Statistical Physics* **95**, 1361–1427 (1999)	June 1998
884	Langford, J. A., and R. D. Moser	Optimal large-eddy simulation formulations for isotropic turbulence—*Journal of Fluid Mechanics* **398**, 321–346 (1999)	July 1998
885	Riahi, D. N.	Boundary-layer theory of magnetohydrodynamic turbulent convection—*Proceedings of the Indian National Academy (Physical Science)* **65A**, 109–116 (1999)	Aug. 1998
886	Riahi, D. N.	Nonlinear thermal instability in spherical shells—in *Nonlinear Instability, Chaos and Turbulence* **2**, 377–402 (1999)	Aug. 1998
887	Riahi, D. N.	Effects of rotation on fully non-axisymmetric chimney convection during alloy solidification—*Journal of Crystal Growth* **204**, 382–394 (1999)	Sept. 1998
888	Fried, E., and S. Sellers	The Debye theory of rotary diffusion	Sept. 1998
889	Short, M., A. K. Kapila, and J. J. Quirk	The hydrodynamic mechanisms of pulsating detonation wave instability—*Proceedings of the Royal Society of London, A* **357**, 3621–3638 (1999)	Sept. 1998
890	Stewart, D. S.	The shock dynamics of multidimensional condensed and gas phase detonations—Proceedings of the 27th International Symposium on Combustion (Boulder, Colo.)	Sept. 1998
891	Kim, K. C., and R. J. Adrian	Very large-scale motion in the outer layer—*Physics of Fluids* **2**, 417–422 (1999)	Oct. 1998
892	Fujisawa, N., and R. J. Adrian	Three-dimensional temperature measurement in turbulent thermal convection by extended range scanning liquid crystal thermometry—*Journal of Visualization* **1**, 355-364 (1999)	Oct. 1998
893	Shen, A. Q., E. Fried, and S. T. Thoroddsen	Is segregation-by-particle-type a generic mechanism underlying finger formation at fronts of flowing granular media?—*Particulate Science and Technology* **17**, 141–148 (1999)	Oct. 1998
894	Shen, A. Q.	Mathematical and analog modeling of lava dome growth	Oct. 1998
895	Buckmaster, J. D., and M. Short	Cellular instabilities, sub-limit structures, and edge-flames in premixed counterflows—*Combustion Theory and Modeling* **3**, 199–214 (1999)	Oct. 1998
896	Harris, J. G.	*Elastic waves*—Part of a book to be published by Cambridge University Press	Dec. 1998
897	Paris, A. J., and G. A. Costello	Cord composite cylindrical shells	Dec. 1998
898	Students in TAM 293–294	Thirty-fourth student symposium on engineering mechanics (May 1997), J. W. Phillips, coordinator: Selected senior projects by M. R. Bracki, A. K. Davis, J. A. (Myers) Hommema, and P. D. Pattillo	Dec. 1998
899	Taha, A., and P. Sofronis	A micromechanics approach to the study of hydrogen transport and embrittlement	Jan. 1999
900	Ferney, B. D., and K. J. Hsia	The influence of multiple slip systems on the brittle–ductile transition in silicon—*Materials Science Engineering A* **272**, 422–430 (1999)	Feb. 1999
901	Fried, E., and A. Q. Shen	Supplemental relations at a phase interface across which the velocity and temperature jump	Mar. 1999
902	Paris, A. J., and G. A. Costello	Cord composite cylindrical shells: Multiple layers of cords at various angles to the shell axis	Apr. 1999
903	Ferney, B. D., M. R. DeVary, K. J. Hsia, and A. Needleman	Oscillatory crack growth in glass—*Scripta Materialia* **41**, 275–281 (1999)	Apr. 1999
904	Fried, E., and S. Sellers	Microforces and the theory of solute transport	Apr. 1999

List of Recent TAM Reports (cont'd)

No.	Authors	Title	Date
905	Balachandar, S., J. D. Buckmaster, and M. Short	The generation of axial vorticity in solid-propellant rocket-motor flows	May 1999
906	Aref, H., and D. L. Vainchtein	The equation of state of a foam	May 1999
907	Subramanian, S. J., and P. Sofronis	Modeling of the interaction between densification mechanisms in powder compaction	May 1999
908	Aref, H., and M. A. Stremler	Four-vortex motion with zero total circulation and impulse—*Physics of Fluids* **11**, 3704-3715	May 1999
909	Adrian, R. J., K. T. Christensen, and Z.-C. Liu	On the analysis and interpretation of turbulent velocity fields—*Experiments in Fluids*, in press (1999)	May 1999
910	Fried, E., and S. Sellers	Theory for atomic diffusion on fixed and deformable crystal lattices	June 1999
911	Sofronis, P., and N. Aravas	Hydrogen induced shear localization of the plastic flow in metals and alloys	June 1999
912	Anderson, D. R., D. E. Carlson, and E. Fried	A continuum-mechanical theory for nematic elastomers	June 1999
913	Riahi, D. N.	High Rayleigh number convection in a rotating melt during alloy solidification—*Recent Developments in Crystal Growth Research*, in press (2000)	July 1999
914	Riahi, D. N.	Buoyancy driven flow in a rotating low Prandtl number melt during alloy solidification—*Current Topics in Crystal Growth Research*, in press (2000)	July 1999
915	Adrian, R. J.	On the physical space equation for large-eddy simulation of inhomogeneous turbulence	July 1999
916	Riahi, D. N.	Wave and vortex generation and interaction in turbulent channel flow between wavy boundaries	July 1999
917	Boyland, P. L., M. A. Stremler, and H. Aref	Topological fluid mechanics of point vortex motions	July 1999
918	Riahi, D. N.	Effects of a vertical magnetic field on chimney convection in a mushy layer—*Journal of Crystal Growth*, in press (2000)	Aug. 1999
919	Riahi, D. N.	Boundary mode–vortex interaction in turbulent channel flow over a non-wavy rough wall	Sept. 1999
920	Block, G. I., J. G. Harris, and T. Hayat	Measurement models for ultrasonic nondestructive evaluation	Sept. 1999
921	Zhang, S., and K. J. Hsia	Modeling the fracture of a sandwich structure due to cavitation in a ductile adhesive layer	Sept. 1999
922	Nimmagadda, P. B. R., and P. Sofronis	Leading order asymptotics at sharp fiber corners in creeping-matrix composite materials	Oct. 1999
923	Yoo, S., and D. N. Riahi	Effects of a moving wavy boundary on channel flow instabilities	Nov. 1999
924	Adrian, R. J., C. D. Meinhart, and C. D. Tomkins	Vortex organization in the outer region of the turbulent boundary layer	Nov. 1999
925	Riahi, D. N., and A. T. Hsui	Finite amplitude thermal convection with variable gravity—*International Journal of Mathematics and Mathematical Sciences*, in press (2000)	Dec. 1999
926	Kwok, W. Y., R. D. Moser, and J. Jiménez	A critical evaluation of the resolution properties of *B*-spline and compact finite difference methods	Feb. 2000
927	Ferry, J. P., and S. Balachandar	A fast Eulerian method for two-phase flow	Feb. 2000

List of Recent TAM Reports (cont'd)

No.	Authors	Title	Date
928	Thoroddsen, S. T., and K. Takehara	The coalescence–cascade of a drop	Feb. 2000
929	Liu, Z.-C., R. J. Adrian, and T. J. Hanratty	Large-scale modes of turbulent channel flow: Transport and structure	Feb. 2000
930	Borodai, S. G., and R. D. Moser	The numerical decomposition of turbulent fluctuations in a compressible boundary layer	Mar. 2000
931	Balachandar, S., and F. M. Najjar	Optimal two-dimensional models for wake flows	Mar. 2000
932	Yoon, H. S., K. V. Sharp, D. F. Hill, R. J. Adrian, S. Balachandar, M. Y. Ha, and K. Kar	Integrated experimental and computational approach to simulation of flow in a stirred tank	Mar. 2000
933	Sakakibara, J., Hishida, K., and W. R. C. Phillips	On the vortical structure in a plane impinging jet	Apr. 2000
934	Phillips, W. R. C.	Eulerian space–time correlations in turbulent shear flows	Apr. 2000
935	Hsui, A. T., and D. N. Riahi	Onset of thermal–chemical convection with crystallization within a binary fluid and its geological implications	Apr. 2000
936	Cermelli, P., E. Fried, and S. Sellers	Configurational stress, yield, and flow in rate-independent plasticity	Apr. 2000
937	Adrian, R. J., C. Meneveau, R. D. Moser, and J. J. Riley	Final report on 'Turbulence Measurements for Large-Eddy Simulation' workshop	Apr. 2000
938	Bagchi, P., and S. Balachandar	Linearly varying ambient flow past a sphere at finite Reynolds number—Part 1: Wake structure and forces in steady straining flow	Apr. 2000
939	Gioia, G., A. DeSimone, M. Ortiz, and A. M. Cuitiño	Folding energetics in thin-film diaphragms	Apr. 2000
940	Chaïeb, S., and G. H. McKinley	Mixing immiscible fluids: Drainage induced cusp formation	May 2000
941	Thoroddsen, S. T., and A. Q. Shen	Granular jets	May 2000
942	Riahi, D. N.	Non-axisymmetric chimney convection in a mushy layer under a high-gravity environment	May 2000
943	Christensen, K. T., S. M. Soloff, and R. J. Adrian	PIV Sleuth: Integrated particle image velocimetry interrogation/validation software	May 2000
944	Wang, J., N. R. Sottos, and R. L. Weaver	Laser induced thin film spallation	May 2000
945	Riahi, D. N.	Magnetohydrodynamic effects in high gravity convection during alloy solidification	June 2000
946	Gioia, G., Y. Wang, and A. M. Cuitiño	The energetics of heterogeneous deformation in open-cell solid foams	June 2000
947	Kessler, M. R., and S. R. White	Self-activated healing of delamination damage in woven composites—*Composites A*, in press (2000)	June 2000
948	Phillips, W. R. C.	On the pseudomomentum and generalized Stokes drift in a spectrum of rotational waves	July 2000
949	Hsui, A. T., and D. N. Riahi	Does the Earth's nonuniform gravitational field affect its mantle convection?	July 2000
950	Phillips, J. W.	Abstract Book, 20th International Congress of Theoretical and Applied Mechanics (27 August – 2 September, 2000, Chicago)	July 2000
951	Vainchtein, D. L., and H. Aref	Morphological transition in compressible foam	July 2000